


## Article

# Electrical Phenomena on Fully Airborne Vertical Electric Antennas in Extreme Weather Conditions

Tomasz Aleksander Miś \*  and Józef Modelski

Warsaw University of Technology, Institute of Radioelectronics and Multimedia Technology,  
ul. Nowowiejska 15/19, 00-665 Warszawa, Poland

\* Correspondence: tomasz.a.mis@mailplus.pl or tomasz.mis.dokt@pw.edu.pl

**Abstract:** This is a conference extension of the paper ‘Investigation on the mature storm cloud’s electric field using long airborne antennas’. The use of vertical antennas (including the VEDs—Vertical Electric Dipoles), lifted up by aerostats to high altitudes without being anchored to the ground, presents numerous advantages in comparison with large terrestrial VLF (Very Low Frequency) antenna structures. A slow-moving floating-earth conductor—a vertical wire antenna—is subjected to intense electrification mechanisms in the atmosphere and inside the cloud layers, producing additional risks for the transmitter and the flight train itself. The electrical potential achieved in this process is, therefore, compared with the flashover voltages over the antenna’s upper fixing point, defining the voltage margins at which the VLF transmitter is able to operate. The electrification processes are also compared to the model based on experimental data on the occurrence of corona discharges over a long, vertical wire traversing a storm cloud layer. The external electric field strength (around the antenna wire) is calculated and compared with older experimental data for storm clouds for various locations, showing the correctness of the proposed analytical electrification model, and, therefore, expanding it with the loss of the electric charge via corona.

**Keywords:** VLF; VED; airborne; balloon; cloud; storm



**Citation:** Miś, T.A.; Modelski, J.

Electrical Phenomena on Fully Airborne Vertical Electric Antennas in Extreme Weather Conditions.

*Energies* **2023**, *16*, 52. <https://doi.org/10.3390/en16010052>

Academic Editors: Meng Huang, Yunxiao Zhang and Chenyuan Teng

Received: 18 November 2022

Revised: 9 December 2022

Accepted: 19 December 2022

Published: 21 December 2022



**Copyright:** © 2022 by the authors. Licensee MDPI, Basel, Switzerland. This article is an open access article distributed under the terms and conditions of the Creative Commons Attribution (CC BY) license (<https://creativecommons.org/licenses/by/4.0/>).

## 1. Introduction

Radio signals below 300 kHz have been successfully employed for the transmission of, e.g., time/frequency standards and military/naval wireless communication with submerged objects. Such signals usually rely on large ground-based antennas with numerous supporting structures, which still have low emission efficiency and high operational costs due to the kilometric/myriametric wavelengths. An emerging solution to these issues is the employment of long, fully airborne (unanchored), vertical antennas, lifted up by aerostats, as shown in Figure 1. This type of antenna also allows placing the transmitter closer to the center of the earth-layer D waveguide of the ionosphere [1,2], giving potentially higher achievable signal ranges while maintaining the vertical polarization of the antenna wire, allowing it to excite stronger electric fields in comparison with aircraft-trailed antennas [3]. As they ascend to their target altitude, devices of this vertical type—which consist of very long (hundreds of meters long) objects classified as ‘floating earth conductors’ [4]—interact intensely with the surrounding atmosphere layers and the objects within them (clouds, mists), posing additional risks to their structures and transmitters. These interactions manifest themselves directly in the form of the changes in the electric field in the environment around the floating conductor, the differentiation of electric charges between the conductor and its surroundings, and the formation of electric discharges in the form of corona and bidirectional discharges [4,5]. These phenomena can be recorded by numerous methods and devices, but some of them—e.g., the measurements of the electric field strength around the conductor/inside the cloud with spherical probes [6]—do not yield undistorted results due to the self-charging of the measuring instruments’ structures [7]. Data obtained indirectly,

i.e., using methods typical for remote sensing in the form of specific radio signatures of specific electrical phenomena [8], allow for an approximate description of the observed phenomena, providing key information both from the perspective of the transmitting antenna (electrical charging speed, possible transmitter overload due to current and voltage pulses, protection against flashovers on the antenna's elements) and the environment (determining the electrical structure of clouds, loss or acquisition of electric charge).



**Figure 1.** An example of a stratospheric balloon antenna—200 m-long VED launched by Warsaw University of Technology, 18 April 2015.

This paper discusses the issue of protection of the fully airborne antenna's elements from two factors:

- Flashovers—voltage discharges over insulating elements (from the electrified antenna wire to the upper elements of the flight train supporting the wire) under various electric fields inside the basic types of clouds, which determine the voltage safety margin for the transmitter's operation;
- The issue of actual corona discharges appearing on the fully airborne antenna wire in relation to the actual external electric fields strength inside the cloud.

An attempt is presented to determine the structure of the electric field of a mature storm cloud on the basis of the obtained radio data on phenomena occurring around a long airborne antenna, which is a problem opposite to electrical analyses determining the design requirements for airborne VLF radio transmitters [9]. The presented model can be used as a verification method for both the proposed theoretical wire electrification processes and the computer simulations, based on numerical solutions of differential equations of individual electrical mechanisms, which require supplementation with real-environment mechanisms (and their orders of magnitude) occurring inside storm clouds [10]. Such mechanisms are difficult to define due to the physical conditions inside the clouds (high intensity of electric fields, potentially destructive discharges, charging of the entire structure of devices instead of dedicated measuring electrodes, etc.).

## 2. Antenna Electrification vs. Insulator Flashover Voltage

The fully airborne, vertical, wire antenna, lifted up by an aerostat, is attached to its flight train (the setup consisting of the parachute, all the tethers, the main gondola, and the payload) by either an insulating tether or an insulating rod. This component has a mushroom-like shield affixed to its upper part in order to reduce the electric field intensity in its proximity, as well as to mechanically protect the attachment point of the wire antenna to the flight train from getting hit by upper flight train components during the re-entry and landing phases of the mission. The design of the insulator and its mushroom-like cap is derived from the original designs tested for use in terrestrial very low frequency (VLF) antenna systems, which defined the flashover voltages for VLF for different insulator lengths, insulator surfaces, and humidity values [11]. For airborne and high-altitude (stratospheric, i.e., >12 km of altitude) conditions, a crucial factor determining the flashover voltage value, apart from the factors mentioned previously, is the atmospheric pressure; the discharge/flashover voltage decreases with this parameter, according to the Paschen's law [12]. Therefore, it is possible to experience corona and flashovers for significantly lower voltages during such flight, which potentially endangers sensitive electronic elements and mechanical components, such as the tethers and the antenna insulator.

The flashover voltage changes in altitude for different environmental conditions—using experimental pressure and temperature data, including a self-heating case, due to the absorption of solar radiation—have been largely described in [13]. This resulted in plots showing the changes of flashover voltage values for two months of the year (collected experimental atmospheric data for December and April) for two main cases: dry and humid. As the electrification processes occur mainly inside the humid environment of the clouds [9], the calculated humid cases can be employed to demonstrate the voltage safety margin for a fully airborne VLF antenna ascending through different kinds of clouds, namely by comparing the total voltage induced on the antenna of given length to the flashover voltage for the given environmental conditions.

The values of the induced electric field strengths for different kinds of clouds have been taken from [9] and recalculated into voltage by multiplying them with the value of the insulator gap of 0.6 m from the cases of humid flashovers from [13]. Figures 2–5 show the comparison of the flashover voltages (upper curves) with the induced voltages on the ascending antenna (lower curves) for the Stratocumulus and Nimbostratus clouds for two wire lengths: 140 m (2022 experiments) and 500 m, for comparative purposes. The 'positive polarization' of the cloud indicates that its upper charge is positive and the lower charge negative; the 'negative polarization' indicates the opposite charge allocation [7]. The Nimbostratus cloud data have their locations of origin indicated (Sankt Petersburg, Kyiv, and Tashkent). An analogue comparison can be made for the mission's descent, where the antenna acquires electric charge up to the touchdown, as shown in Figures 6–9, also for antenna lengths of 140 m and 500 m. 'KULLA 3' denotes the cases where the antenna material absorbs the solar radiation and heats itself up (experiments executed in April, approx. twice the temperature values from the colder case). The blue curves, showing the

flashover voltage changes with altitude for the December atmospheric data, begin with an offset in values due to the data registration start at the altitude of 65 m.

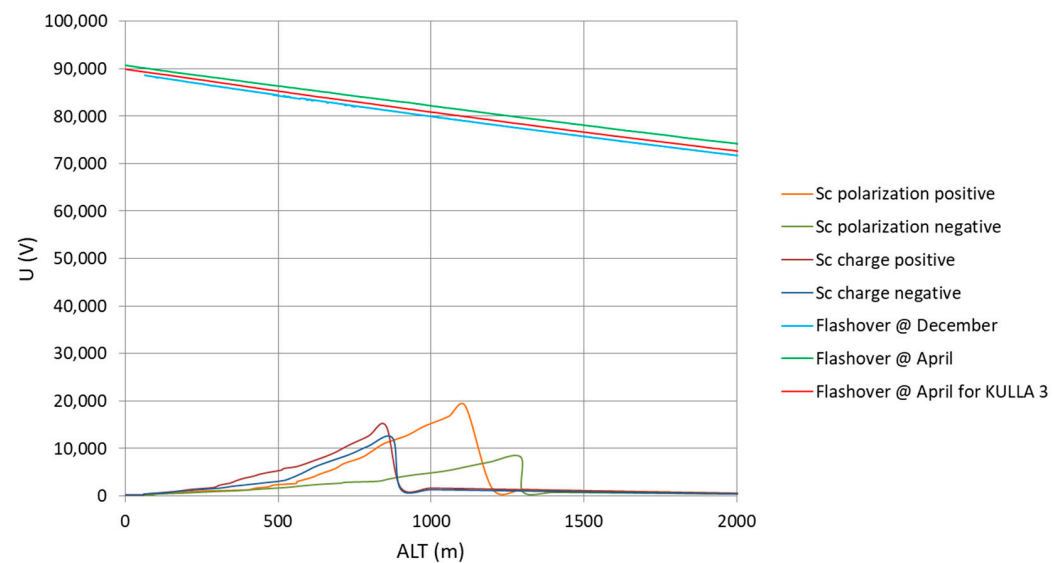


**Figure 2.** The flashover and induced voltage through the Stratocumulus clouds on the 140 m-long fully airborne antenna during the ascent.

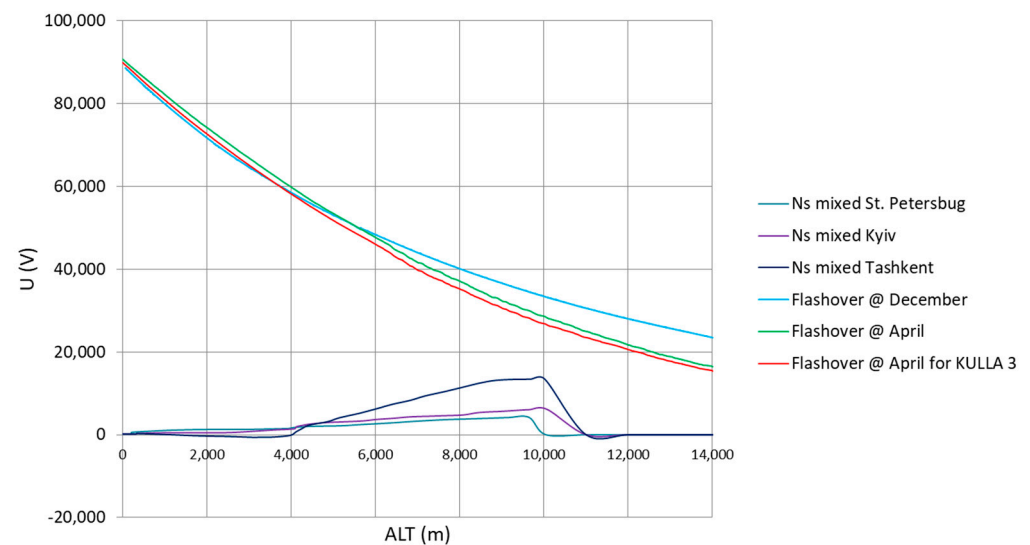


**Figure 3.** The flashover and induced voltage through the Nimbostratus clouds on the 140 m-long fully airborne antenna during the ascent.

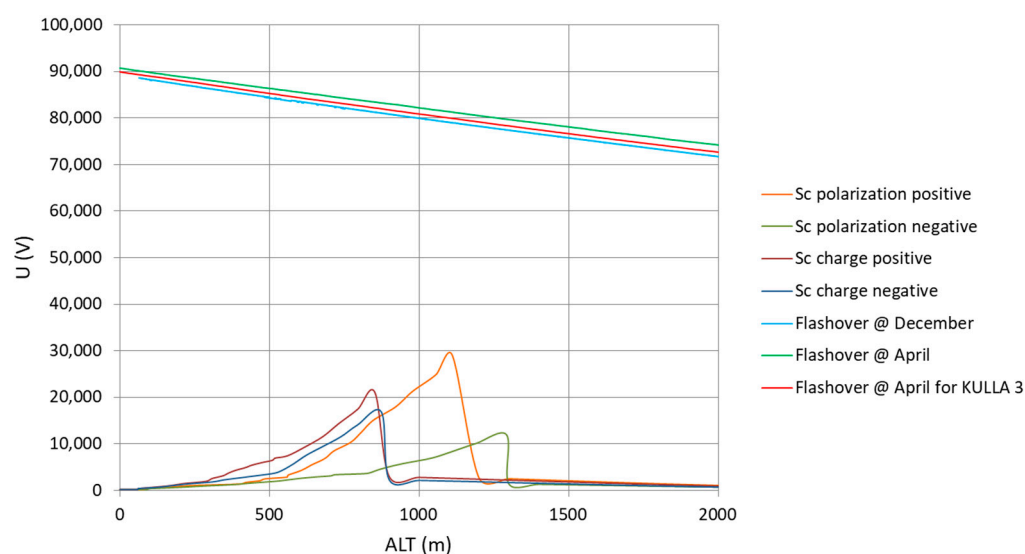


**Figure 4.** The flashover and induced voltage through the Stratocumulus clouds on the 500 m-long fully airborne antenna during the ascent.

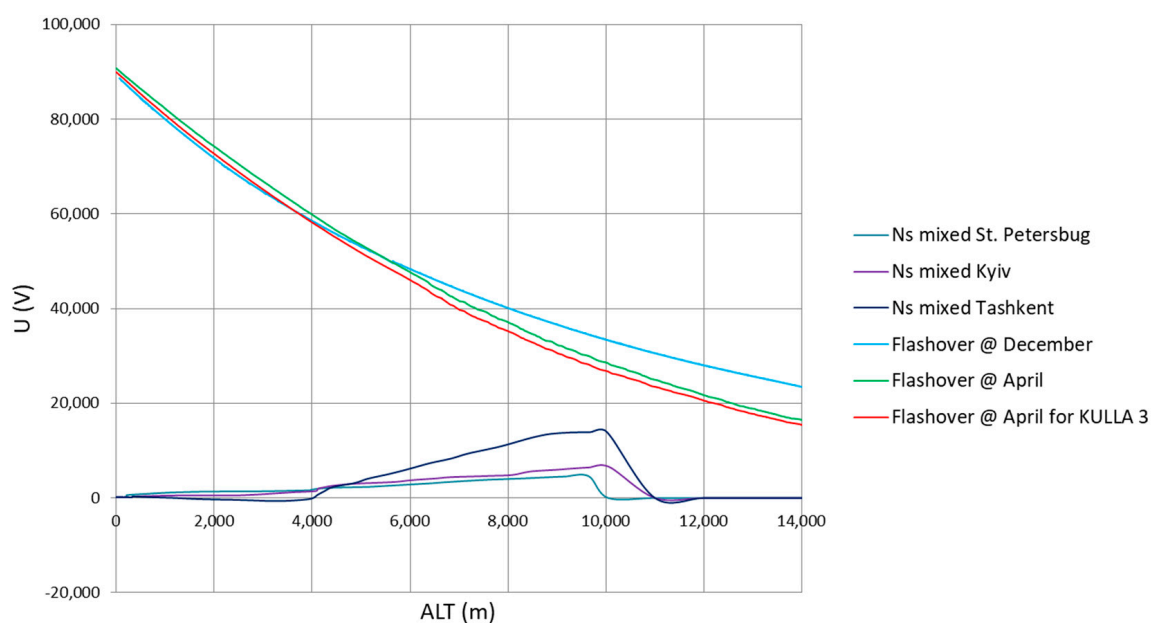


**Figure 5.** The flashover and induced voltage through the Nimbostratus clouds on the 500 m-long fully airborne antenna during the ascent.

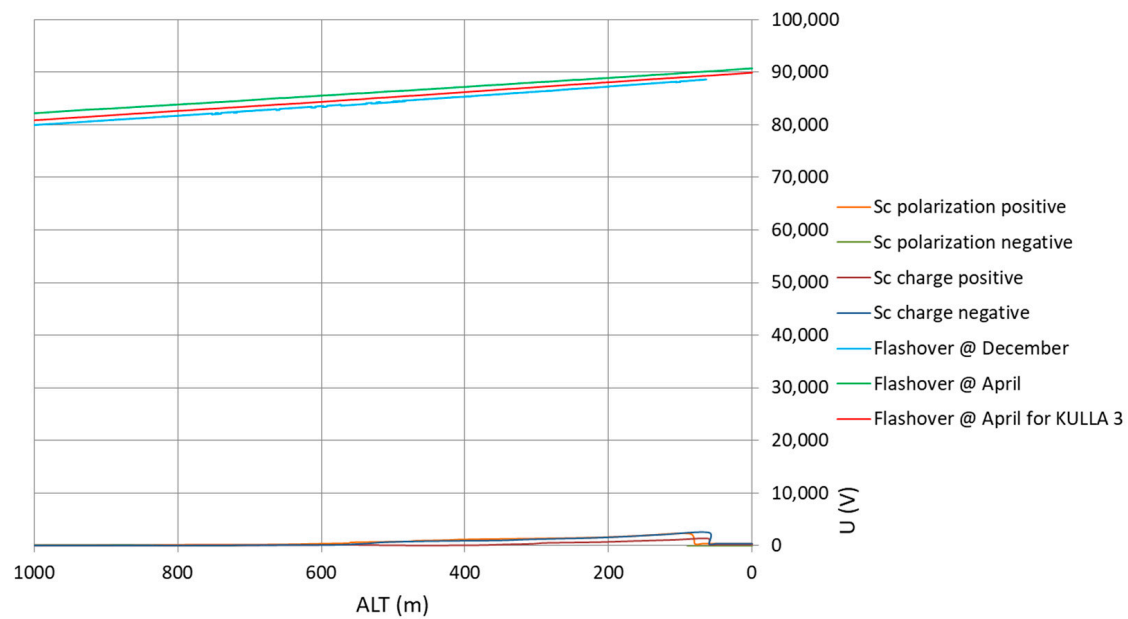


**Figure 6.** The flashover and induced voltage for the re-entry through the Stratocumulus clouds on the 140 m-long fully airborne antenna.

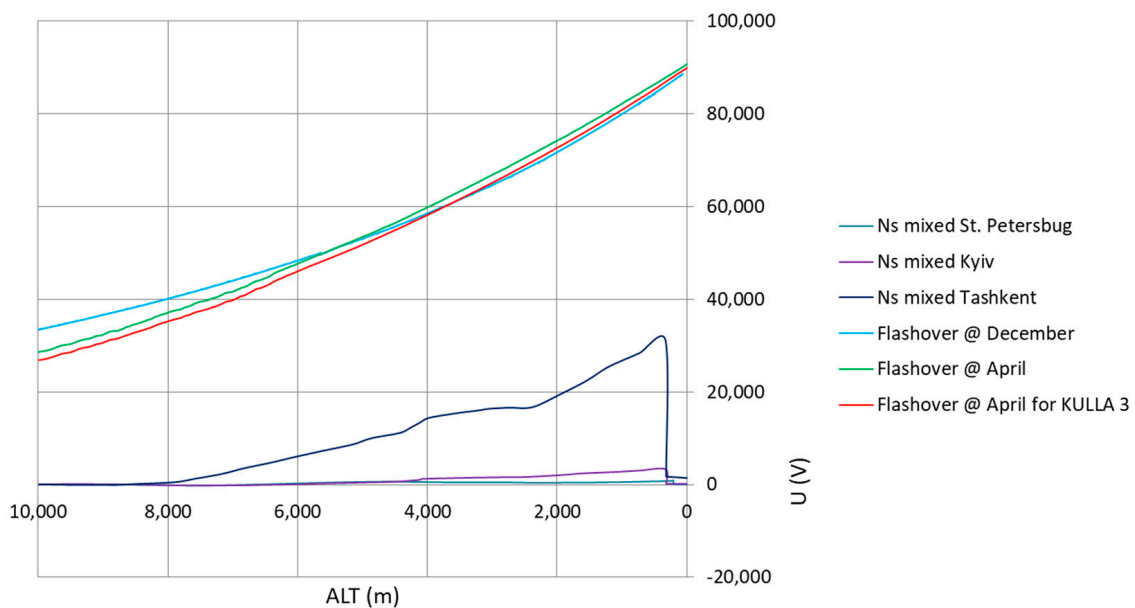


**Figure 7.** The flashover and induced voltage for the re-entry through the Nimbostratus clouds on the 140 m-long fully airborne antenna.

Table 1 shows the minimum obtainable peak voltage margins, read from the calculated electrification (i.e., the antenna's electrical charging in flight) vs. flashover voltage cases. The values decrease with the antenna's length (more precisely, with the logarithm of the length [9]) and present the smallest margins for the worst electrification cases, the Nimbostratus (layered storm-type) clouds. For the Stratocumulus (layered heap-type) clouds, the smallest margins are reached to the positively polarized (charged + in the upper part and – in the lower part) cloud cases.

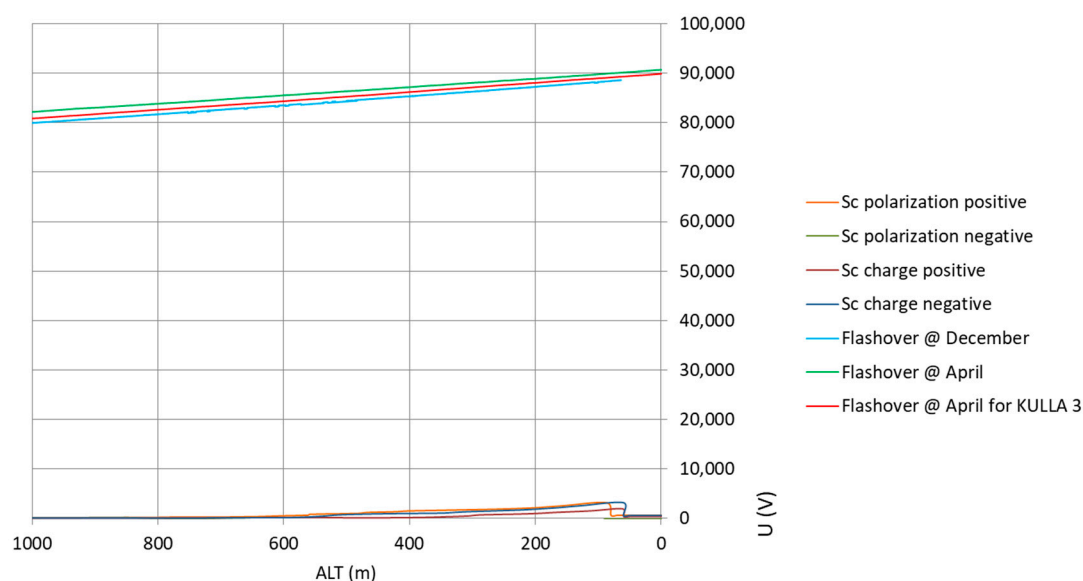


**Figure 8.** The flashover and induced voltage for the re-entry through the Stratocumulus clouds on the 500 m-long fully airborne antenna.

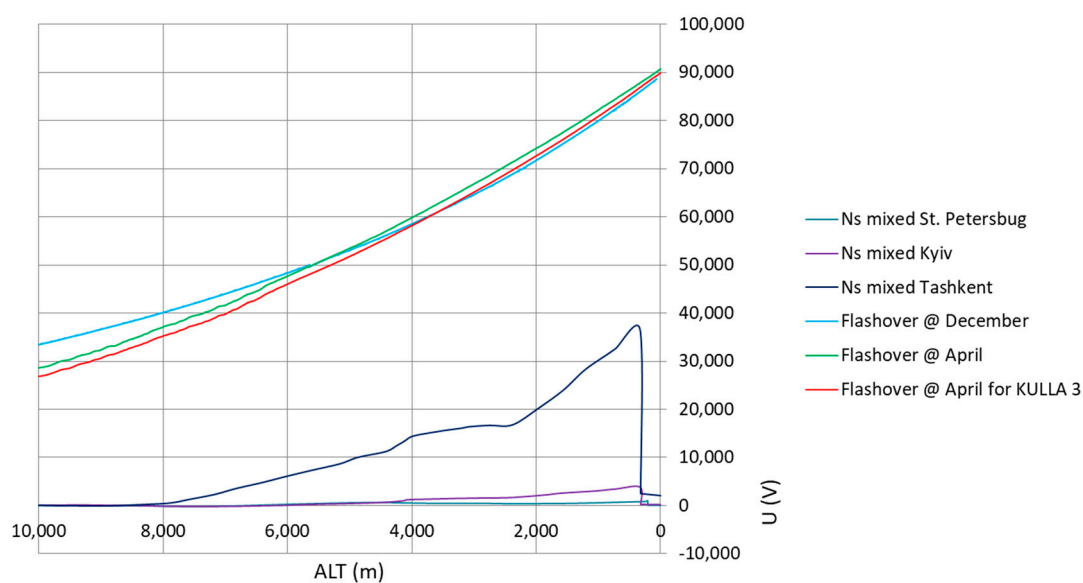


**Figure 9.** The flashover and induced voltage for the re-entry through the Nimbostratus clouds on the 500 m-long fully airborne antenna.

**Table 1.** Minimum obtainable peak voltage margins due to electrification processes and flashover limits for a fully airborne vertical VLF antenna of two lengths.

Peak Voltage Margins [kV]—The Ascent			
140 m		500 m	
Stratocumulus	Nimbostratus	Stratocumulus	Nimbostratus
61	13.15	50	12.4
Peak Voltage Margins [kV]—The Descent			
140 m		500 m	
Stratocumulus	Nimbostratus	Stratocumulus	Nimbostratus
87.5	57.35	85.45	50.35

### 3. Antenna's Actual Corona Recalculation into Electric Field Structure

The most intense electrification processes, resulting in the smallest margin for the antenna's peak transmitting voltage, appear for the Nimbostratus cloud cases, with the Tashkent case producing the strongest induced electric field around the antenna wire. Due to the heterogeneity of the insides of the cloud, the electric field in microscopic proximity to the antenna may reach the values at which the corona is induced, regardless of the calculated flashover voltage due to Paschen's law. This is consistent with past experiments, which indicated the existence of corona on free-floating conductor-type antennas [14] and anchored very long antennas, operating at VLF frequency range [5]. The elicitation of corona is facilitated with the increase of the electric charge, proportional to the antenna's dimensions and the cloud type. Therefore, for fixed cloud type, antenna geometry, and analytically known mechanism of electrification, the estimation of the natural electric field values and structure changes with altitude can be estimated, if data on experimental corona discharges are collected.

The corona discharges—recorded as voltage/current signals—have the form of impulse-like signals, appearing in repetitive intervals, depending on the magnitude of the electric charge transferred and the form of the conductors on which the corona is incepted [15]. Popular methods for indirect (i.e., with no electrical/galvanic connection between the recording circuit and the element-incepting corona) registration of this phenomena include the recording of its radio signatures, usually with bandwidth reaching tens of kHz [8]. In 2015, a 225 kHz AM radio receiver was placed in the middle of a fully airborne, 200 m-long, stratospheric balloon antenna, but did not deliver any useful data due to an internal malfunction [16]. A similar experiment was performed in 2021, with the radio receiver operating at 144 kHz AM (below the broadcasting part of the low-frequency spectrum), which delivered recorded acoustic signals associated with the corona impulses appearing on the 140 m-long antenna wire passing through a Nimbostratus cloud in a warm storm front [17]. The recorded impulses did not appear before the launch of the antenna (when the receiver was positioned on the ground), nor when the mission entered the Altostratus layer of the storm front, leaving the storm cloud below.

Every corona impulse transfers a given amount of electric charge [18]. Assuming that the electric field strength at which the corona impulse is triggered ( $E_{gr.}$ ) is set at the tropospheric value of 2.7 kV/m often employed in engineering calculations [19], the amount of electric charge transferred per impulse is indicated by the electric field strength after the impulse. The higher this value is, the lower the electric charge transferred. As the data delivered in the 140 m-long antenna experiment was present in the form of normalized (between 0 and 1) amplitude values in time [9], the electric field strength after the subsequent corona impulses can be described as  $E_{gr.}A_i$ , where  $A_i$  is the impulse amplitude recorded in the experiment. Figure 9 describes the electric field strength function in time  $E(t)$  for subsequent corona impulses (at the time moments  $t_i$  and  $t_{i+1}$ ). The electrification mechanisms inside a storm cloud, investigated experimentally, allow the increase in the electric field strength after a discharge back to the values preceding the discharge in a few seconds only [7]. For the corona, the impulses—functioning as minor discharges—appear in short intervals between each other, such that the increase of the electric field strength in time between them would take the practical form of linear functions (as in Figure 10).

Between the subsequent corona discharges for  $t_i$  and  $t_{i+1}$ , the electric field resulting from this linear charging process ( $E_{charging}$ ) can be described as [16]:

$$E_{charging} = E_{gr.} \left[ A_i + \frac{1 - A_i}{t_{i+1} - t_i} t \right] \quad (1)$$

As this increase of the electric field strength around the antenna wire (length  $2c = 140$  m and thickness  $b = 10^{-4}$  m) is caused by the electrification mechanism inside a storm

cloud with the charging velocity  $v_C = 0.3 \text{ nC/m}^3/\text{s}$ , the electrification function described in [9] can be applied for the same time interval:

$$E_{\text{charging}} = E_{\text{ext.}} + \frac{3E_{\text{ext.}}}{4\pi r} \left[ \log \frac{a+c}{a-c} \right] \left( 1 - e^{-\frac{bv_C}{3E_{\text{ext.}}\epsilon_0}t} \right) \quad (2)$$

where  $t$  [s] is the time variable (to be calculated from a known ascent velocity and given altitude data),  $\epsilon_0$  is the electrical permittivity of the medium,  $E_{\text{ext.}}$  [V/m] is the external (primordial) electric field inside the cloud,  $r$  [m] is the distance between the cloud and the wire (assumed as an averaged value of 1 m due to the lack of a pair of solid electrodes), and  $a$  [m] is the product of a square root of a sum of cubes of  $r$  and  $c$ .

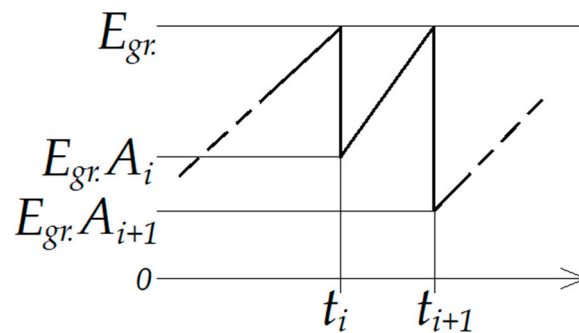


**Figure 10.** The schematic  $E(t)$  plot of the corona discharge model inside the cloud.

As Equation (2) was formulated for a case where the electric charge does not leave the antenna due to the corona discharges [9], the model (1) expands this case towards the conditions where the corona appears when traversing the cloud. If Equations (1) and (2) are compared to each other, the calculation of  $E_{\text{ext.}}$  is possible [16], with the additional parameters  $f_G$  and  $f_C$  introduced to simplify the final expression:

$$E_{\text{ext.}} = \frac{f_C}{W_k \left( -\frac{f_G f_C e^{-\frac{(f_G+1)f_C}{E_{\text{charging}}}}}{E_{\text{charging}}} \right) + f_G f_C + f_C} \quad (3)$$

$$f_G = \frac{3 \log \left[ \frac{a+c}{a-c} \right]}{4\pi r} \quad (4)$$

$$f_C = \frac{bv_C t}{3\epsilon_0} \quad (5)$$

where  $W_k$  is the Lambert W function calculated for the  $k = 0$  branch (as the values of the function's argument are the small and negative,  $< -1$ ).

Figures 11 and 12 present the calculated  $E_{\text{ext.}}$  values for the time values  $0.5(t_{i+1} - t_i)$ , ascent velocity of 3 m/s, and 2 altitude (ALT) ranges of the balloon mission, where the corona discharges have been recorded inside the Nimbostratus cloud. The functions appear as highly oscillating due to the fact that the electric field strength inside the cloud is highly influenced by a slow-moving, large metallic object (the antenna), while the cloud tends to keep its electrical equilibrium; the electric field strength rises rapidly after each discharge [7,9]. Above 1500 m, the frequency of appearance of the corona discharges decreased due to the lower electric field values inside the cloud. Figure 13 shows the comparison of the calculated external electric field strength with older experimental data from three locations (Sankt Petersburg, Kyiv, and Tashkent) [7], aligned to the comparable altitudes (the 2020 Nimbostratus case began at lower altitudes). The calculated  $E_{\text{ext.}}$  function can be approximated by a 4th degree polynomial to estimate the electric field strength without the disturbing metallic object; the maximum values reached exceed

1300 V/m, situating the function in the middle of the older experimental electric field strength ranges.

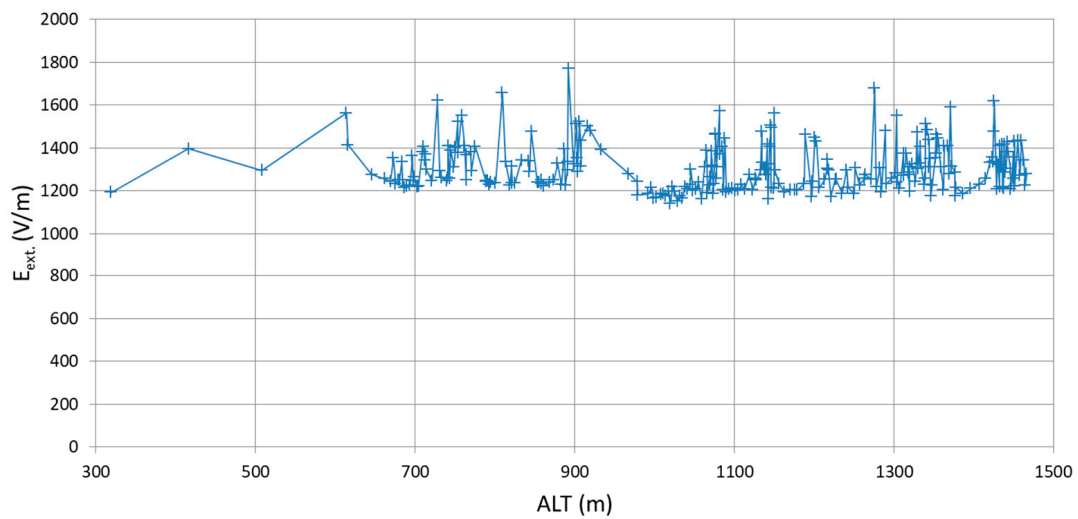


**Figure 11.** The calculated (by Equation (3)) external electric field strength  $E_{ext.}$  for the altitudes between 300 and 1500 m.

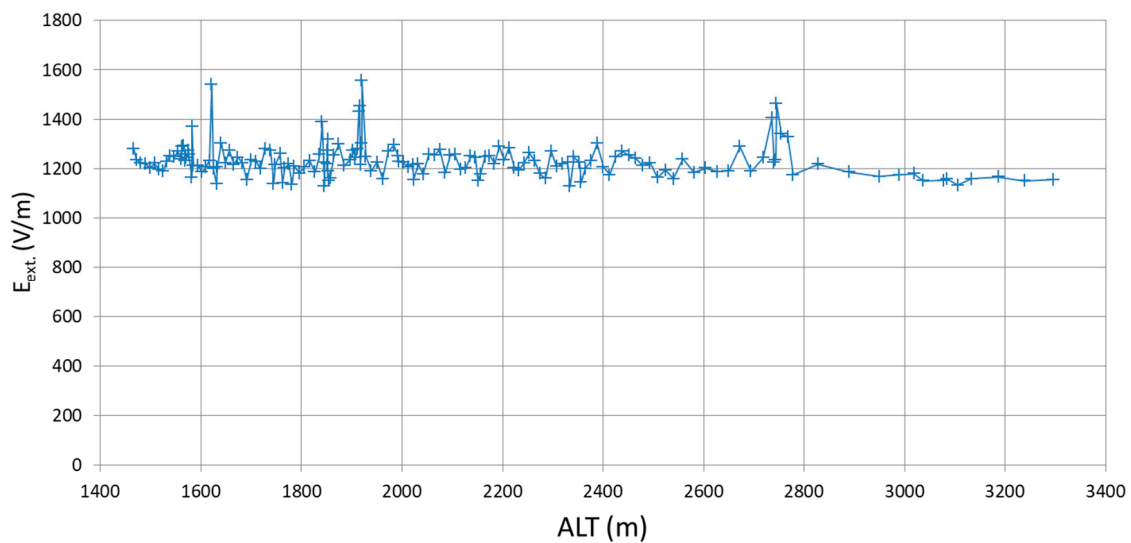


**Figure 12.** The calculated (by Equation (3)) external electric field strength  $E_{ext.}$  for the altitudes between 1500 and 3400 m.

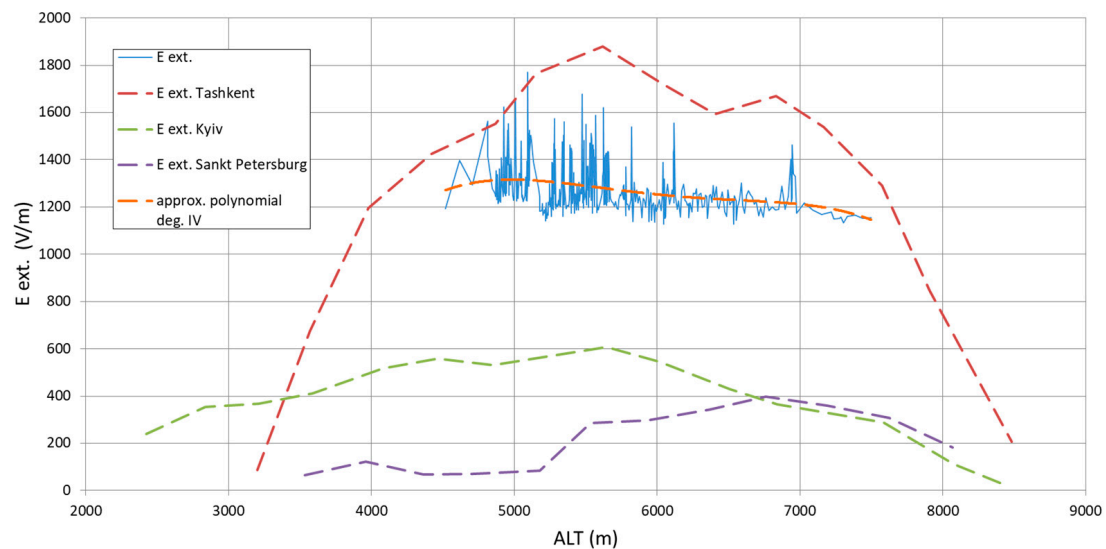


**Figure 13.** The comparison between electric field strengths in storm clouds from different locations.

#### 4. Discussion

In the general approach, the VLF transmitting systems operating in the range of kW require high voltages in their antenna circuits [20]. To minimize the risk of corona during the ascent phase of such fully airborne transmitting systems, the chosen peak antenna voltage must fit within the ranges indicated in Table 1. The worst cases determined in this analysis indicate that the minimum available transmitter peak voltage (voltage margin) appears for 500 m-long radiators at storm conditions and reach 12.4 kV, a value that decreases with the logarithm of the antenna's length, as with the antenna's length, the induced electric field strength increases towards the values at which the flashovers appear. The smallest peak voltage margin for the storm clouds appeared, however, for a single location (Tashkent), with the Kyiv and Sankt Petersburg locations presenting significantly higher voltage margins. The calculated external electric field strength for the 2020 experiment, plotted in Figure 12, shows that these values are positioned between the Tashkent and Kyiv locations, which would result in peak voltage margins comparable to those calculated for the Tashkent case ( $<15$  kV). Naturally, from the perspective of flight organization and flight mechanics, the storm cloud flight case bears the most difficulties and risks, and a launch in these conditions should be avoided if possible.

The descents of the fully airborne antennas (under a parachute) present very high peak voltage margins for the Stratocumulus clouds ( $>85$  kV), which offer a high level of safety and a possible increase of transmitter power. For the Nimbostratus cases, the minimal voltage margin (found for the Tashkent case) decreases to a value slightly above 50 kV for the 500 m-long antenna. The margins, similar to the ascent cases, decrease with the increasing length of the antennas due to the intensifying electrification processes. From the perspective of flight planning and execution, the descent phases are characterized by a moderate controllability of the flight train (i.e., the flight train—the antenna, the gondola etc.—may not be able to avoid entering a storm cloud when descending under a parachute). Therefore, for this flight stage, higher available voltage margins increase the corona safety level for a transmitter operating at higher powers.

The calculation of the external electric field strength from the experimental corona discharges' data has delivered results in agreement with older experimental data (the dataset for each location is an average over multiple cases—10 to 72 for the Stratocumulus and 7 to 18 for the Nimbostratus [7]). This shows the correct approach to the constructed analytical models. Therefore, in the overall investigation of the electrification of fully airborne balloon antennas, the proposed model of the electric field's increase between

the subsequent corona discharges can be used with the electrification model as a way of incorporating the electric charge loss due to corona discharges.

## 5. Conclusions

This paper presented two aspects crucial for the safety of operation of a freely airborne VLF antenna system in various cloud conditions, including the worst case scenarios of flights in storms—the voltage margins, produced as results of comparing flashover voltages to voltages gained via the electrification of the antenna wire, and the recreation of the electric field strength around the antenna inside a storm cloud for given experimental data on the corona discharges. The indicated minimal voltage margins for different antenna lengths, different types of clouds, and different flight phases have been shown, presenting length- and cloud-type-related tendencies. These voltages will be useful in determining maximum operational transmitter voltages that define the maximum fully airborne VLF transmitter power for different mission profiles and mission phases. The presented electrification model involving corona discharges allowed the calculation of the electric field strength around the antenna inside the storm cloud, giving results comparable to older experimental data, verifying the employed theoretical mechanism of antenna electrification, and introducing the theoretical model of the electric field strength increase with simultaneous corona discharges, which will be useful for further modelling of large antenna/balloon structures traversing various cloud layers.

**Author Contributions:** Conceptualization, T.A.M.; methodology, T.A.M.; validation, T.A.M.; formal analysis, T.A.M.; investigation, T.A.M.; resources, T.A.M.; data curation, T.A.M.; writing—original draft preparation, T.A.M.; writing—review and editing, T.A.M.; visualization, T.A.M.; supervision, J.M. All authors have read and agreed to the published version of the manuscript.

**Funding:** Part of the experiments featured in this article were sponsored by the companies Nasiona Wronkowski and Saaten Union.

**Data Availability Statement:** Not applicable.

**Acknowledgments:** This article is an expanded version of the paper presented at the National Conference on Radiocommunication, Radio Broadcasting and Television (KKRRiT) 2022, 7–9 September, Warsaw, Poland.

**Conflicts of Interest:** The authors declare no conflict of interest.

## References

- Burrows, M.L. *ELF Communications Antennas*; Peter Peregrinus Ltd.: London, UK, 1978.
- Miś, T.A. The concept of an airborne VLF transmitter with vertical electric dipole antenna. In Proceedings of the 2018 IEEE International Symposium on Antennas and Propagation & USNC/URSI National Radio Science Meeting, Boston, MA, USA, 8–13 July 2018. [\[CrossRef\]](#)
- Galejs, J. VLF fields of elevated sources. *Radio Sci.* **1970**, *5*, 1163–1168. [\[CrossRef\]](#)
- Pavan, C.; Fontanes, P.; Urbani, M.; Nguyen, N.C.; Martinez-Sanchez, M.; Peraire, J.; Montanya, J.; Guerra-Garcia, C. Aircraft Charging and its influence on triggered lightning. *J. Geophys. Res. Atmos.* **2019**, *125*, e2019JD031245. [\[CrossRef\]](#)
- Crawford, R.L.; Jordan, K.L. Tethered Aerostat VLF/LF Transmitter System Design Considerations. In Proceedings of the AGARD Conference: ELF/VLF/LF Radio Propagation and System Aspects, Brussels, Belgium, 28 September–2 October 1992; 1992.
- Jaworek, A. *Measurement Methods of the Electrostatics*; Institute of Fluid-Flow Machinery, Polish Academy of Sciences: Gdańsk, Poland, 1985.
- Imianitov, I.M.; Chubarina, E.V.; Shwarts, J.M. *The Electricity of Clouds*; National Scientific Publisher: Warsaw, Poland, 1974.
- Florkowski, M. Partial discharges in high-voltage insulating systems. In *Mechanisms, Processing and Analytics*; AGH University of Science and Technology Press: Kraków, Poland, 2020.
- Miś, T.A.; Modelski, J. In-Flight Electromagnetic Compatibility of Airborne Vertical VLF Antennas. *Sensors* **2022**, *22*, 5302. [\[CrossRef\]](#) [\[PubMed\]](#)
- Doshi, N.A.; Agashe, S.D. Modelling of ions for seeding technique to electrify the atmosphere. *J. Electrostat.* **2015**, *75*, 19–26. [\[CrossRef\]](#)
- Brown, W.W. Radio frequency tests on antenna insulators. *Proc. Inst. Radio Eng.* **1923**, *11*, 495–522. [\[CrossRef\]](#)
- Babikov, M.A.; Komarov, N.S.; Sergeyev, A.S. *High Voltage Technology*; WN-T: Warsaw, Poland, 1967.

13. Miś, T.A. Flashover Analysis of Near-Space Antenna Mounting Insulators. In Proceedings of the 13th European Conference on Antennas and Propagation (EuCAP), Kraków, Poland, 31 March–4 April 2019.
14. Hall, W.C. Electrostatic dischargers for aircraft. *J. Appl. Phys.* **1947**, *18*, 759–765. [[CrossRef](#)]
15. Sugimoto, T.; Kikuchi, H.; Higashiyama, Y. Positive discharge from a grounded electrode toward negatively charged particles cloud. *J. Electrostat.* **2005**, *63*, 609–614. [[CrossRef](#)]
16. Miś, T.A. Investigation on the mature storm cloud's electric field using long airborne antennas. In Proceedings of the National Conference on Radiocommunication, Radio Broadcasting and Television KKRRiT, Warsaw, Poland, 7–9 September 2022.
17. Schmidt, M. *Meteorology*; WKiŁ: Warsaw, Poland, 1975.
18. Miki, M.; Rakov, V.A.; Shindo, T.; Diendorfer, G.; Mair, M.; Heidler, F.; Zischrank, W.; Uman, M.A.; Thottappillil, R.; Wang, D. Initial stage in lightning initiated from tall objects and in-rocket-triggered lightning. *J. Geophys. Res. Atmos.* **2005**, *110*, D2. [[CrossRef](#)]
19. Masewicz, T.; Wenda. *Radio Technology Material Engineering*; WKiŁ: Warsaw, Poland, 1973.
20. Watt, A.D. *VLF Radio Engineering*; Pergamon Press Inc.: Oxford, UK, 1967.

**Disclaimer/Publisher's Note:** The statements, opinions and data contained in all publications are solely those of the individual author(s) and contributor(s) and not of MDPI and/or the editor(s). MDPI and/or the editor(s) disclaim responsibility for any injury to people or property resulting from any ideas, methods, instructions or products referred to in the content.